The Role of Polydopamine Films in the Immobilization of Aggregates of TiO2 Nanoparticles on Gold and ITO Surfaces

applied sciences

MDPI

Article

The Role of Polydopamine Films in the Immobilization of Aggregates of TiO_2 Nanoparticles on Gold and ITO Surfaces

Andrea Atrei [1,*], Maddalena Corsini [1], Giuseppe Di Florio [2], Simonetta Muccifora [3], Silvia Spriano [4], Sara Ferraris [4], Simone Pepi [1] and Jozsef Toth [5]

[1] Dipartimento di Biotecnologie, Chimica e Farmacia, Università di Siena, 53100 Siena, Italy; maddalena.corsini@unisi.it (M.C.); simone.pepi@unisi.it (S.P.)
[2] ENEA-Italian National Agency for New Technologies, Energy and Sustainable Economic Development, Casaccia Research Centre, 00124 Rome, Italy; giuseppe.diflorio@enea.it
[3] Dipartimento di Scienze della Vita, Università di Siena, 53100 Siena, Italy; simonetta.muccifora@unisi.it
[4] Dipartimento di Scienza Applicata e Tecnologia-DISAT, Politecnico di Torino, 10129 Torino, Italy; silvia.spriano@polito.it (S.S.); sara.ferraris@polito.it (S.F.)
[5] HUN-REN Institute for Nuclear Research, H-4026 Debrecen, Hungary; toth.jozsef@atomki.hu
* Correspondence: atrei@unisi.it

Abstract

In the present work, we investigated the role of polydopamine coatings in anchoring TiO_2 P25 nanoparticles on gold and ITO surfaces. For this purpose, we studied the adhesion of polydopamine-coated aggregates of TiO_2 nanoparticles on bare substrates and of aggregates of bare TiO_2 nanoparticles on polydopamine-coated substrates. Coating with polydopamine was accomplished by oxidation in air of alkaline aqueous dopamine solutions in which the nanoparticles or the substrates were immersed. Dynamic light scattering, Fourier transform infrared spectroscopy, and transmission electron microscopy were used for the chemical and morphological characterization of aggregates of the nanoparticles. The adhesion of aggregates of the nanoparticles on the substrates was evaluated by means of AFM and XPS. The results of this study suggest that the adhesion of TiO_2 P25 nanoparticles on polydopamine films, as well as of polydopamine-coated TiO_2 P25 nanoparticles, is a balance of several contributions: chemical interactions, electrostatic interactions, and coating roughness. Electrostatic attraction and repulsion between nanoparticles and the substrate appear to play an important role, as indicated by the ζ-potential values of nanoparticles and substrates.

Keywords: polydopamine; TiO_2; Au; ITO; nanoparticles; AFM; XPS

1. Introduction

Since the first paper in 2007 [1], polydopamine (PDA) in the form of coatings, films, or nanoparticles (NPs), as well as its properties and mechanisms of adhesion, has been the subject of thousands of publications [2–5]. This interest is motivated by the simple coating procedure and the ability of PDA to adhere to virtually any surface. Moreover, PDA-coated surfaces have potential applications in many fields ranging from chemical sensors to biomaterials [6,7]. PDA NPs and films can be easily prepared by oxidation of dopamine in alkaline aqueous solutions. Less attention has been paid to the use of PDA to anchor NPs of other materials on solid surfaces. In some works, PDA is used as an intermediate layer modified with specific molecules to bind NPs. For instance, a substrate was coated with PDA and subsequently functionalized with polyethyleneimine to capture Au NPs [8].

Received: 16 July 2026
Revised: 19 August 2026
Accepted: 24 August 2026
Published: 27 August 2026

The various functional groups on the surface of PDA films and NPs (amine, catechol, and quinone groups) can bind metal ions [9]. In the case of noble metal ions, such as Ag^+ and Au^{3+}, PDA reduces them to form metal NPs adhering to the PDA surface [10]. Even without any surface modification, the functional groups of PDA films should be able to bind polymer, metal, and metal oxide NPs. Thus, PDA could work as a "glue" either by coating the substrate or by coating the NPs. In our previous studies, we found that the adhesion of magnetite NPs on gold surfaces depends on the conditions used to prepare the coating [11,12]. The preparation conditions of the coatings, particularly the dopamine concentration and the reaction time, affect the chemical composition and morphology of the PDA layers. These two aspects play an important role in determining the capability of PDA films to anchor NPs [11–14]. The adhesion of metal oxide NPs on PDA films and of PDA-coated NPs is the result of a subtle balance of specific chemical interactions as well as of electrostatic attraction. The complex heterogeneous nature of PDA films, constituted by different types of building units, hampered a complete structural determination [15–17]. This lack of information renders difficult the computational studies of the PDA/substrate interface to understand the contributions to the adhesion [18]. In the present study, we investigated the effect of PDA coating on the immobilization of TiO_2 NPs on gold and indium tin oxide (ITO) surfaces. The aim of the work is to shed light on the various contributions, particularly chemical and electrostatic interactions, to the adhesive properties of PDA coatings. We studied the adhesion of bare and PDA-coated TiO_2 P25 NPs on clean gold and ITO substrates, as well as of bare TiO_2 P25 NPs on ITO substrates modified with PDA films. In the present work, the term TiO_2 NPs indicates aggregates of individual NPs, since the results of this study concern the adhesion of aggregates of TiO_2 NPs. Indeed, dynamic light scattering (DLS) shows that, under our experimental conditions, in the aqueous dispersions, there are aggregates of TiO_2 NPs. The adhesion of TiO_2 NPs was monitored by means of atomic force microscopy (AFM) and X-ray photoelectron spectroscopy (XPS). In order to clarify the role of electrostatic interaction between the NPs and the substrates, the surface ζ-potentials of the gold and ITO surfaces used in the experiments were measured. We chose P25 TiO_2 as oxide NPs, since these NPs, modified with PDA, exhibit interesting photocatalytic and electro-photocatalytic properties [19–22].

2. Materials and Methods

2.1. Materials

Dopamine hydrochloride (DA) (≥99% purity) was purchased from Fisher Scientific (Hampton, NH, United States). Titanium dioxide (TiO_2) P25 nanopowder, with an average primary particle size of approximately 20 nm, was obtained from PlasmaChem (PlasmaChem GmbH, Berlin, Germany). As gold substrates, gold-coated silicon samples (50 nm thick Au films) cut from a p-type Si wafer, oriented along the (100) plane (Electron Microscopy Sciences, Hatfield, PA, USA), were used. For the deposition on ITO, silica glass samples coated with ITO films (thickness 100 nm) (Ossila Ltd., Sheffield, UK) were employed.

2.2. Characterization of the Samples by DLS, FTIR, Surface ζ-Potential, AFM, XPS and TEM

A Zetasizer Nano ZS90 instrument (Malvern, UK) was used to perform Dynamic Light Scattering (DLS) and ζ-potential measurements. Hydrodynamic diameters are expressed as Z-average values. ζ-potential values were calculated by applying the Smoluchowski equation. NPs were dispersed in double-distilled water (DDW) (pH around 6.5) and the pH was adjusted to acidic or basic values by adding droplets of HCl or NaOH solutions as needed. The concentration of all samples was on the order of 0.05 mg/mL, and the measurements were performed at 25 °C. The reported values of the hydrodynamic diameter

and of the polydispersity index (PDI) are averages of three sets of acquisitions. The dispersions were sonicated for 30 min before DLS measurements. Surface ζ-potential measurements were performed on gold and ITO substrates by means of an electrokinetic analyzer (SurPASS, Anton Paar, Graz, Austria) equipped with an adjustable gap cell. Two titration curves were measured on the gold substrate. A first curve was measured from pH 5.5 to pH 3, adding 0.05 M HCl to the 0.001 M KCl electrolyte solution through the automatic titration unit of the instrument, and then from pH 5.5 to pH 8, adding 0.05 M NaOH. The second titration curve was obtained by moving firstly from pH 5.5 toward the basic region and then toward the acidic region. A set of samples was used to obtain each titration curve. The two curves were compared to identify any possible irreversible surface reaction during pH titration and to check the reproducibility of the results. In the case of the ITO substrate, surface ζ-potential was measured for 50 min at pH 7.4 in diluted Simulated Body Solution (SBF). SBF was added drop by drop to the 0.001 M KCl electrolyte solution until pH 7.4 and an electrical conductivity of 15 mS/m were obtained. For ITO, surface potential measurements were performed at neutral pH, since in acidic and basic enviroments, there is a corrosion of the ITO substrate. Infrared spectra were acquired by means of an Alpha II FTIR spectrometer (Bruker), operated in Attenuated Total Reflection (ATR) mode, equipped with a diamond crystal. Each spectrum was obtained by averaging 64 scans in the range of 400–4000 cm^{-1}. AFM images were acquired using a Solver P47-PRO SPM (NT-MDT) microscope. Images were collected in semi-contact mode with a silicon tip. The force constant of the cantilever was ca. 20 N/m and the oscillating frequency was 200 kHz. The roughness of the surfaces (arithmetic and root mean square values) and the surface coverages of the adhered NPs were determined by using the software of the microscope. Surface coverages were estimated by measuring the ratio of the area occupied by the NPs and of the scanned area of the substrate. The particles present in the image were identified by setting a threshold value of the height. Scans of 20 μm × 20 μm were analyzed to determine roughness and surface coverage values. AFM measurements were repeated on different zones of the samples to obtain the average values of surface coverage reported in the text. XPS measurements were performed in an ultra-high vacuum chamber equipped with a homemade hemispherical electron energy analyzer and a non-monochromatized Al Kα X-ray source. The angle between the direction of the photon beam and the axis of the analyzer was 70°. Photoelectrons were collected in the direction normal to the surface. The XPS spectra were acquired in the fixed retarding ratio mode. The binding energy (BE) scale was calibrated by setting the aliphatic component of the C1s peak to 285.0 eV. Transmission electron microscopy (TEM) images were acquired using a FEI Tecnai G2 Spirit microscope operated at an accelerating voltage of 100 kV. Bare TiO_2 NPs and PDA-coated TiO_2 NPs (prepared with 0.5 mg/mL and 2.0 mg/mL DA concentrations) were deposited by drop-casting diluted aqueous dispersions on grids covered by Formvar.

2.3. Preparation of PDA/TiO_2 P25 NPs

A total of 100 mg of TiO_2 NPs were dispersed in 100 mL of phosphate buffer solution (0.05 M, pH 8.0) prepared from $H_2PO_4^-$/HPO_4^{2-} salts. The dispersion was sonicated for 10 min to ensure proper dispersion of the NPs. Different concentrations of DA (0.25, 0.5, 1.0, and 2.0 mg/mL) were added to the suspension to investigate the influence of DA concentration on the coating properties. To initiate dopamine oxidation and polymerization, air was bubbled into the suspension. The reaction flask was protected from light by wrapping it in aluminum foil. The polymerization reaction was carried out overnight (~16 h) at room temperature (25 °C). This reaction time was long enough to guarantee a complete coating of the NPs. Then, PDA/TiO_2 NPs were separated by centrifugation,

washed several times with DDW to remove excess reactants and loosely bound polymer, and then dried under a nitrogen gas flux.

2.4. Coating of ITO Substrates with PDA

ITO surfaces were coated with PDA films by immersing the ITO surfaces in a $H_2PO_4^-/HPO_4^{2-}$ buffer solution at pH 8.0, containing 1 mg/mL of DA. The reaction was carried out at room temperature for one hour, with air bubbling into the solution. Afterwards, the sample was rinsed with DDW and dried under a flux of N_2.

2.5. Deposition of Bare and PDA-Coated TiO_2 NPs on Gold and ITO Substrates

Gold-coated silicon substrates were cleaned by immersion in a piraña solution and extensively rinsed with DDW. ITO-coated silica glass substrates were washed with acetone to remove surface contamination. NPs were deposited on the two substrates by immersing the samples in dispersions (1 mg/mL) of TiO_2 NPs in DDW at neutral pH for 1 h under shaking, at room temperature. After this treatment, the samples were washed with DDW to remove the NPs that did not adhere to the substrate and dried under N_2 flux.

3. Results and Discussion

3.1. Characterization of Bare and PDA-Coated TiO_2 P25 NPs

The results of the DLS measurements performed on aqueous dispersions of bare and PDA-coated TiO_2 NPs at neutral pH are reported in Table 1. The hydrodynamic diameter of the TiO_2 NPs (Table 1) is much larger than the size of the individual NPs, which is ca. 20 nm. This is an indication that TiO_2 NPs form large aggregates in aqueous dispersions at neutral pH, which are not destroyed by sonication. The decrease in size after PDA coating, prepared with a DA concentration below 0.5 mg/mL, can be explained by partial disaggregation of the NP clusters due to DA adsorption on their surface. At the basic pH used to prepare the PDA coating, TiO_2 NPs have a relatively high-magnitude ζ-potential (ca. −40 mV). This produces a larger electrostatic repulsion between NPs, compared to that at neutral pH, which prevents their aggregation. The ζ-potential of bare TiO_2 P25 NPs at neutral pH (about +20 mV) is larger than that expected on the basis of the point of zero charge (PZC) values reported in the literature for TiO_2 P25, which are centred around 6 [23]. The presence of residual impurities originating from the preparation process may be responsible for the relatively high ζ-potential of the TiO_2 P25 NPs used in this work [24]. Indeed, the XPS analysis of the TiO_2 P25 NPs revealed the presence of nitrogen at the surface of the NPs (Figure S1, Supplementary Materials). The BEs of the components of the N1s are close to those of nitrogen atoms adsorbed on TiO_2 and of interstitial nitrogen atoms in TiO_2 [25]. The surface coverage of nitrogen atoms was estimated to be ca. 0.2 monolayer (see Supplementary Materials). These species at the surface of the TiO_2 P25 NPs, even if present at monolayer or sub-monolayer levels, could contribute to increasing the ζ-potential compared to pure TiO_2. The most relevant result of this analysis is the change in sign of the ζ-potential upon coating the NPs with PDA. Only small changes in ζ-potential are observed by varying the concentration of DA used in the coating preparation. The coating of the NPs with PDA was monitored by FTIR spectroscopy. The spectra measured for increasing amounts of DA used for the coating are shown in Figure 1.

The comparison of the spectra with that of PDA NPs indicates that TiO_2 P25 NPs are coated with PDA. The small differences (mainly of the relative peak intensities) in the spectra passing from 0.25 to 2 mg/mL concentration of DA reveal some changes in the composition of the PDA layer. The largest, broad band around 1500–1600 cm^{-1} has many overlapping contributions of the building blocks of PDA [26–29]. Hence, the various components cannot be univocally identified by a curve fitting analysis. The shoulder

around 1700 cm^{-1} (more clearly visible in the spectrum of NPs prepared with 2 mg/mL of DA) can be assigned to the C=O stretching of quinone groups in PDA. It is noteworthy that the variations with DA concentration for PDA/TiO_2 are smaller than those observed for PDA/Fe_3O_4 [12]. TEM images of bare and PDA-coated TiO_2 P25 NPs are shown in Figure 2. Bare TiO_2 P25 NPs (Figure 2a) appear as small aggregates and show prismatic shapes consistent with those reported for anatase NPs [30,31]. NPs have sharp edges even when aggregated. The shapes of the NPs can be associated with 2D projections of truncated bipyramids of anatase crystals, delimited by (101) and (001) facets. NPs have a distribution of sizes between 10 and 30 nm. The PDA coating around the TiO_2 cores can be distinguished from the oxide NPs because it is more transparent to electrons than oxide NPs and its edges are more rounded (Figure 2b,c). Upon increasing the DA concentration used to prepare the coating, there is an increase in the average thickness, which is around 10 nm when the DA concentration is 2.0 mg/mL. The image of PDA-coated Fe_3O_4 NPs is shown in Figure 2d for comparison. In the case of magnetite NPs, the PDA coating (prepared under the same conditions as for TiO_2, with 2 mg/mL DA) is significantly thicker and the coating edges are smoother [12]. These differences can be attributed to the oxidation of DA induced by the reduction of Fe(III) to Fe(II) at the surface of magnetite NPs. The redox process is expected to produce different intermediate species of oxidized DA, compared to the case of TiO_2 NPs, influencing the growth kinetics of the PDA coating.

Table 1. Hydrodynamic diameter, polydispersity index (PDI) and ζ-potential of bare TiO_2 P25 NPs and PDA-coated TiO_2 P25 NPs samples. The concentration of DA used to prepare the PDA coating is reported in brackets. Measurements were performed at pH 6.5.

Sample	Hydrodynamic Diameter (nm)	PDI	ζ-Potential (mV)
TiO_2 P25 NPs	288 ± 10	0.15 ± 0.01	23 ± 3
PDA/TiO_2 NPs (0.25 mg/mL)	213 ± 5	0.32 ± 0.04	−36 ± 2
PDA/TiO_2 NPs (0.5 mg/mL)	186 ± 5	0.18 ± 0.02	−33 ± 2
PDA/TiO_2 NPs (1.0 mg/mL)	222 ± 10	0.19 ± 0.02	−32 ± 2
PDA/TiO_2 NPs (2.0 mg/mL).	345 ± 15	0.19 ± 0.03	−29 ± 2

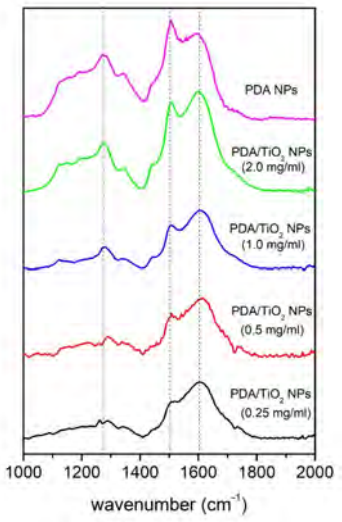

Figure 1. FTIR spectra of the samples of PDA/TiO_2 and PDA NPs.

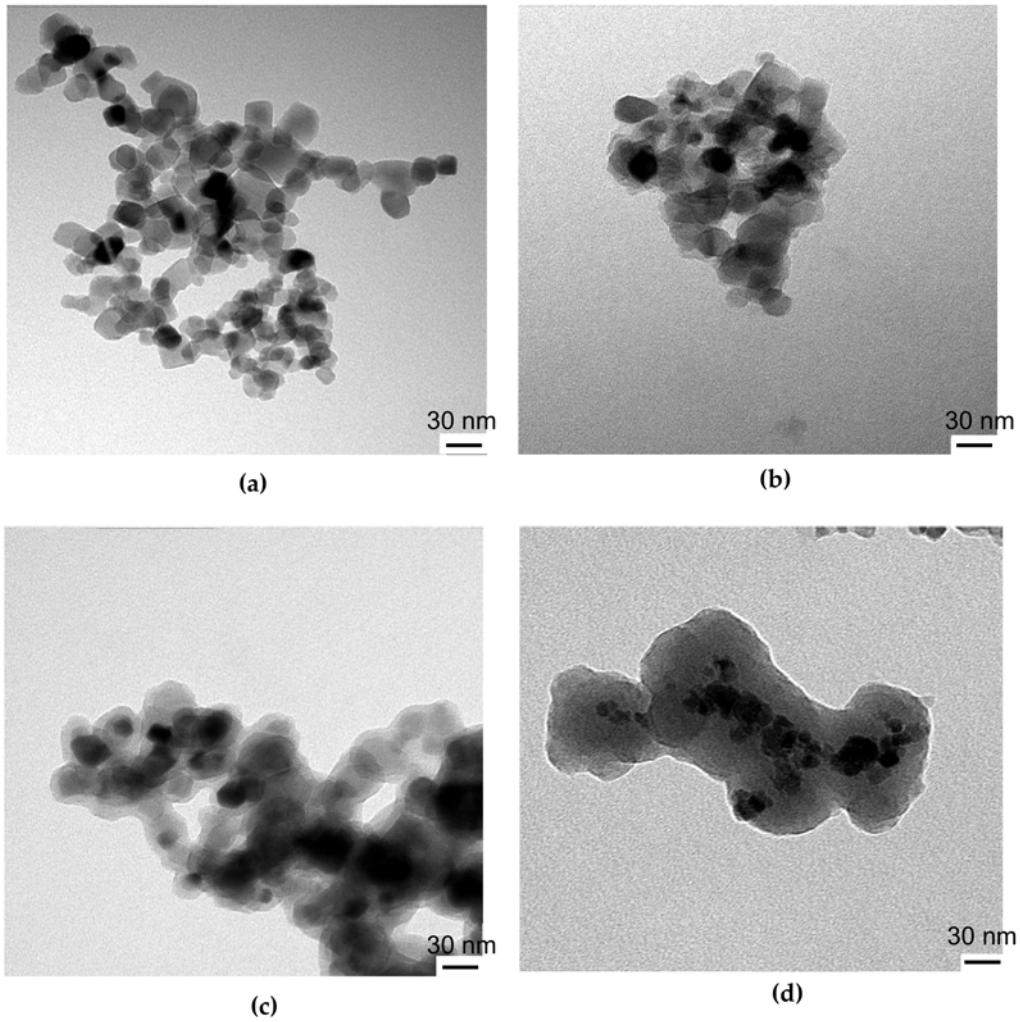

Figure 2. TEM images of bare TiO_2 NPs (**a**), PDA/TiO_2 NPs prepared with 0.5 mg/mL of DA (**b**), PDA/TiO_2 NPs prepared with 2.0 mg/mL of DA (**c**), and PDA/Fe_3O_4 NPs prepared with 2.0 mg/mL of DA (**d**).

3.2. AFM of Bare and PDA-Coated TiO_2 P25 NPs on Gold

AFM images show that TiO_2 P25 NPs can be deposited on gold surfaces by dip-coating in an aqueous dispersion of the NPs (Figure 3a). The roughness values of the various surfaces are reported in Table S1, Supplementary Materials. TiO_2 NPs are present as rather large aggregates which do not cover the gold substrate evenly. By measuring the fraction of substrate area occupied by the TiO_2 P25 NPs, it is possible to estimate a surface coverage of ca. 45%. It is conceivable that electrostatic attraction is responsible, to a large extent, for the adhesion of TiO_2 NPs on gold, as was found in the case of γ-Fe_2O_3 NPs on Au [32].

This hypothesis is confirmed by the surface ζ-potential measurements of the gold substrate (Figure S2, Supplementary Materials). At neutral pH, the gold substrate has a negative ζ-potential (−70 mV), in agreement with the data reported in the literature [33]. The negative potential can be attributed to the spill-over of electrons producing an electric dipole with the negative end towards the outside of the solid. It is worth noting that Fe_3O_4 NPs, which have a lower ζ-potential (+13 mV) than TiO_2 NPs, do not adhere to gold surfaces [11]. TiO_2 NPs acquire negative ζ-potentials (ca. −50 mV) after treating them with a NaOH solution (pH 11) and thorough rinsing with DDW. The surface coverage of these NPs with negative ζ-potential is drastically reduced compared to that of TiO_2 NPs having a positive ζ-potential. A low coverage is obtained also by dip-coating from solution at pH 11 (See Table 2). The surface coverage of the TiO_2/Au sample prepared by dip-coating at

neutral pH is reduced after washing with a NaOH solution at pH 11. On the other hand, the surface coverage does not change significantly by carrying out the NP deposition at acidic pH (See Table 2).

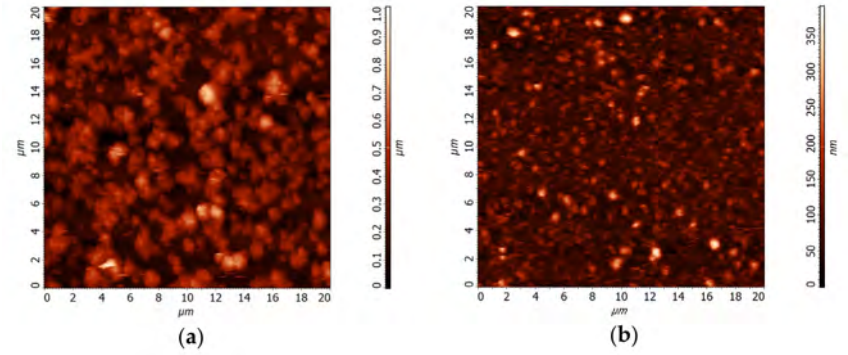

Figure 3. AFM images of bare TiO_2 NPs deposited by dip-coating on gold from a dispersion at neutral pH (**a**), and of PDA/TiO_2 NPs (DA concentration: 0.5 mg/mL) deposited by dip-coating on gold at pH 3 (**b**).

Table 2. ζ-potential (mV) of the TiO_2 P25 NPs and surface coverage (%) at various pH values.

pH	ζ-Potential (mV)	Surface Coverage (%)
3	42 ± 2	54 ± 10
6.5	23 ± 3	45 ± 15
11	−49 ± 2	8 ± 2

The deposition by dip-coating on Au substrates of PDA/TiO_2 NPs prepared with various DA concentrations was investigated by AFM. When the NPs were deposited from dispersions at neutral pH, rather small surface coverages were found (see Table 3). As discussed in ref. [12] the adhesion of PDA-coated Fe_3O_4 NPs is the result of various contributions, particularly the chemical composition and irregular shapes of the PDA-coated TiO_2 NPs. The FTIR spectra of PDA/TiO_2 NPs are very close to those of PDA NPs in the entire range of the DA concentration (see Figure 1) and to those of PDA/Fe_3O_4 prepared with 2.0 mg/mL of DA. All these NPs, which seem to have the same composition, do not stick (or they do, but to a less extent) on gold surfaces. The changes in composition can affect, in turn, the roughness or, more correctly, the morphology at nanometric scale of the PDA coating, as observed by TEM for PDA/Fe_3O_4 NPs [12].

Table 3. Surface coverages (%) estimated by AFM of PDA/TiO_2 NPs deposited on Au at pH 6.5 and 3. The DA concentrations used to coat the TiO_2 NPs are reported.

Sample	pH 6.5	pH 3
PDA/TiO_2 NPs (0.25 mg/mL DA)	15 ± 4	52
PDA/TiO_2 NPs (0.5 mg/mL DA)	5 ± 2	53
PDA/TiO_2 NPs (1.0 mg/mL DA)	1 ± 1	51
PDA/TiO_2 NPs (2.0 mg/mL DA)	4 ± 1	27

Significantly larger surface coverages are achieved when the dip-coating deposition is carried out from dispersions at pH 3 (see Table 3 and Figure 3b). The PDA/TiO_2 NPs uniformly cover the gold surface. The adhesion of PDA/TiO_2 NPs on gold can be explained considering that PDA/TiO_2 NPs are positively charged at acidic pH (due to protonation of residual -NH_2 groups) as indicated by the ζ-potential around +30 ÷ +40 mV. The data in Table 3 show that the pH of the dispersion plays the most important role in determining the adhesion of the PDA/TiO_2 NPs. However, other contributions, for instance the irregular shape of the PDA coating, can affect the surface coverage. The positively charged NPs adhere to the gold surface, which is negatively charged due to the electron spillover. It is remarkable that the surface coverage is not significantly reduced after an overnight immersion of the samples in DDW. This behaviour is difficult to explain in terms of just electrostatic attraction since protonation/deprotonation processes should be almost instantaneous. A tentative explanation is a change in the conformation of the PDA layer at acid pH which exposes units capable to adhere to the substrate surface. Since the structural rearrangement of the polymer is expected to be a slow process, PDA-coated TiO_2 NPs remain attached when the pH is brought back to neutrality. However, it must be stressed that this is only a hypothesis which might be verified in future studies by using, for instance, a quartz microbalance with dissipation monitoring technique.

3.3. AFM of Bare and PDA-Coated TiO_2 NPs on ITO

As in the case of gold surfaces, TiO_2 P25 NPs adhere to ITO surfaces when deposited by dip-coating from dispersions at neutral pH, as shown by AFM (Figure 4a). Surface coverages estimated for the various samples by analyzing AFM images are reported in Table 4. TiO_2 P25 NPs remain attached to the surface even after prolonged washing and they can be removed only by sonication. TiO_2 P25 NPs, which after treatment with NaOH solution acquire a negative ζ-potential (−18 mV), do not stick to the ITO substrate. Since ITO has a negative surface ζ-potential at neutral pH (ca. −80 mV, see Figure S2, Supplementary Materials), we can conclude that the electrostatic attraction is responsible for the adhesion of TiO_2 P25 NPs on the ITO substrate.

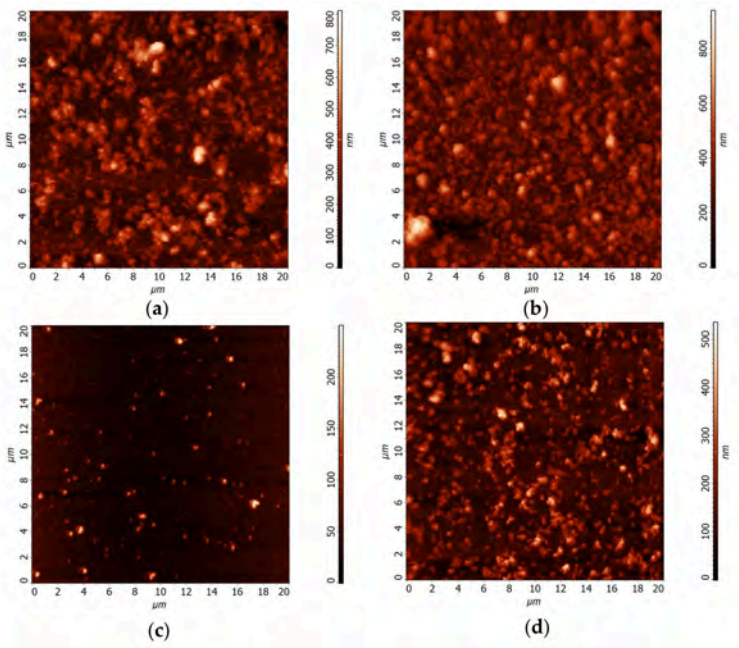

Figure 4. (**a**) Bare TiO_2 P25 NPs deposited on ITO. (**b**) PDA-coated TiO_2 P25 NPs (DA conc. 0.5 mg/mL) deposited on ITO. (**c**) PDA films on ITO. (**d**) Bare TiO_2 P25 NPs deposited on PDA-coated ITO surface.

Table 4. Surface coverages (%) of bare TiO_2 P25 NPs deposited on ITO and PDA/ITO, and PDA-coated P25 NPs (DA conc. 0.5 mg/mL) on ITO, as determined by AFM. For bare TiO_2 P25 NPs on ITO and PDA/ITO, the surface coverages determined by XPS are reported.

Sample	Surface Coverage (AFM)	Surface Coverage (XPS)
TiO_2 NPs on ITO	37 ± 7	29 ± 5
TiO_2 NPs on PDA/ITO	25 ± 8	18 ± 5
PDA/TiO_2 NPs on ITO	37 ± 10	N/A

N/A: Not Available. Measurements were not performed for this sample.

PDA-coated TiO_2 P25 NPs stick on ITO with a surface coverage equal to that of bare NPs (Figure 4b and Table 4). The adhesion occurs despite both the NPs and the substrate having a negative ζ-potential. Hence specific, chemical interactions are relevant for the adhesion of PDA-coated TiO_2 P25 NPs. PDA films were deposited on ITO to investigate the sticking of TiO_2 P25 NPs on these surfaces. A typical AFM image of PDA films on ITO is shown in Figure 4c. PDA films appear to coat the entire substrate with sparse islands having heights up to a few hundred nm. Similar results were obtained for PDA films deposited on a gold surface [11]. The formation of islands separated by flat regions was observed by AFM for PDA films deposited under various conditions and substrates [13,26,34]. AFM images of PDA/ITO substrates immersed in dispersions of TiO_2 P25 NPs exhibit a substantial increase in island density, indicating the sticking of the NPs to the PDA film (Figure 4d). The surface coverage determined by AFM in this case is expected to be overestimated, since a fraction of the observed protrusions is due to PDA islands of the coating. The surface coverage of TiO_2 P25 NPs is lower on the PDA film than on the ITO surface. The lower coverage can be ascribed to the difference in the magnitude of the electrostatic interaction or to the PDA film roughness.

3.4. XPS Determination of Surface Coverage of TiO_2 P25 NPs

Surface coverages determined by AFM may differ from the actual values due to AFM tip convolution effects [35,36]. The finite size of the tip is likely to result in an overestimation of the lateral extension of the islands of the deposited material. Surface coverages determined by XPS or other surface analysis methods are expected to be more accurate than those estimated by AFM. Nonetheless, analysis of AFM images acquired under similar experimental conditions can provide reliable results about relative trends in surface coverage [37,38]. Samples of TiO_2 P25 NPs deposited on ITO and PDA/ITO substrates were investigated by means of XPS to obtain an independent estimation of surface coverage. The Ti2p XPS spectra measured for bare TiO_2 P25 NPs and for NPs deposited on ITO and PDA/ITO surfaces are shown in Figure S3, Supplementary Materials. Since the size of the TiO_2 NPs is much larger than the attenuation length of photoelectrons (2–3 nm), the ratio of the Ti2p intensities measured for NPs deposited on the two substrates, and for a thick layer of NPs on an adhesive tape, is proportional to the surface coverage (see Supplementary Materials). The results of the XPS analysis are reported in Table 4. The uncertainty in the XPS analysis is mainly due to the different amounts of surface contamination on the analyzed samples. Although the surface coverages determined by AFM are 20–30% larger than those obtained by XPS, the results of the two analyses give the same trend.

4. Conclusions

The properties of PDA as an adhesive layer to anchor aggregates of TiO_2 P25 NPs on gold and ITO surfaces were investigated by means of FTIR, ζ-potential, AFM, and XPS. The results of this study indicate that the adhesion of TiO_2 P25 NPs on PDA films, as

well as that of PDA-coated TiO_2 P25 NPs, is a balance of several contributions: chemical interactions, electrostatic interactions, coating roughness of the substrates, and the morphology of the aggregates. Electrostatic attraction and repulsion between the NPs and the substrates appear to play a relevant role as indicated by the ζ-potential of the NPs and of the substrates. By varying the pH of the dispersions from which the NPs were deposited, it is possible to control the surface coverage of the NPs. The surface coverages of TiO_2 NPs determined by AFM were overestimated compared with those obtained by XPS, but both techniques provide the same trends. The possibility to anchor TiO_2 P25 NPs on conductive substrates is relevant for photoelectrochemical applications, exploiting the PDA layer as a photosensitizer.

Supplementary Materials: The following supporting information can be downloaded at https://www.mdpi.com/article/10.3390/app16178513/s1, Figure S1: XPS N1; Figure S2: ζ-potential Au and ITO surfaces; Figure S3: XPS Ti2p. Table S1: Roughness analysis of the AFM images of the various samples.

Author Contributions: Conceptualization, A.A., M.C., and G.D.F.; methodology, A.A., M.C., and G.D.F.; investigation, A.A., S.M., S.S., S.F., S.P., and J.T.; writing—original draft preparation, A.A., M.C., G.D.F., S.S., and S.M.; funding acquisition, A.A. All authors have read and agreed to the published version of the manuscript.

Funding: The authors thank the Ministero dell'Ambiente e della Sicurezza Energetica (SOLE-H2, Project RSH2A_000004-CUP: F57G25000080006), funded by the European Union—NextGenerationEU, Piano Nazionale di Ripresa e Resilienza (PNRR) Missione 2 Componente 2 Investimento 3.5-D.D. 279 05/08/2025.

Institutional Review Board Statement: Not applicable.

Informed Consent Statement: Not applicable.

Data Availability Statement: The data presented in this study are available on request from the corresponding author.

Conflicts of Interest: The authors declare no conflicts of interest.

References

1. Lee, H.; Dellatore, S.M.; Miller, W.M.; Messersmith, P.B. Mussel-inspired surface chemistry for multifunctional coatings. *Science* **2007**, *318*, 426–430. [CrossRef] [PubMed]
2. Liu, Y.; Ai, K.; Lu, L. Polydopamine and its derivative materials: Synthesis and promising applications in energy, environmental, and biomedical fields. *Chem. Rev.* **2014**, *114*, 5057–5115. [CrossRef] [PubMed]
3. Ball, V. Polydopamine Nanomaterials: Recent Advances in Synthesis Methods and Applications. *Front. Bioeng. Biotechnol.* **2018**, *6*, 109. [CrossRef] [PubMed]
4. Saiz-Poseu, J.; Macebo-Aracil, J.; Nador, F.; Busqu´e, F.; Ruiz-Molina, D. The chemistry behind catechol-based adhesion. *Angew. Chem. Int. Ed.* **2019**, *58*, 696–714. [CrossRef] [PubMed]
5. Szewczyk, J.; Radhakrishnan, D.; Łukasiewicz, Z.; Coy, E. Review on polydopamine supramolecular ordering–mechanism elucidation and application in 2D nanocomposites fabrication. *Eur. Polym. J.* **2024**, *221*, 113530. [CrossRef]
6. Rocha, J.; Hasimoto, L.H.; Santhiago, M. Recent Progress and future perspective of polydopamine nanofilms toward functional electrochemical sensors. *Anal. Bioanal. Chem.* **2023**, *415*, 3799–3816. [CrossRef] [PubMed]
7. Shlapakova, L.E.; Surmeneva, M.A.; Surmenev, R.A. Polydopamine-based multifunctional biomaterials: Strategies for controlling redox and photothermal properties for biomedical applications. *Int. J. Biol. Macromol.* **2026**, *354*, 15128. [CrossRef] [PubMed]
8. Chae, W.R.; Song, Y.; Lee, N.Y. Polydopamine-mediated gold nanoparticle coating strategy and its application in photothermal polymerase chain reaction. *Lab Chip* **2025**, *25*, 1429–1438. [CrossRef] [PubMed]
9. Li, H.; Jia, Y.; Bai, S.; Peng, H.; Li, J. Metal-chelated polydopamine nanomaterials: Nanoarchitectonics and applications in biomedicine, catalysis, and energy storage. *Adv. Colloid Interface Sci.* **2024**, *334*, 103316. [CrossRef] [PubMed]
10. Liu, S.; Qileng, A.; Huang, J.; Gao, Q.; Liu, Y. Polydopamine as a bridge to decorate monodisperse gold nanoparticles on Fe_3O_4 nanoclusters for the catalytic reduction of 4-nitrophenol. *RSC Adv.* **2017**, *7*, 45545–45551. [CrossRef]

11. Atrei, A.; Chokheli, S.; Corsini, M.; Tóth, J.; Di Florio, G. Uptake of Magnetite Nanoparticles on Polydopamine Films Deposited on Gold Surfaces: A Study by AFM and XPS. *Nanomaterials* **2024**, *14*, 1699. [CrossRef] [PubMed]
12. Corsini, M.; Di Florio, G.; Polvani, A.; Toth, J.; Atrei, A. Sticking of magnetite nanoparticles coated with dopamine and polydopamine on gold substrates. *Colloids Surf. A.* **2025**, *711*, 136377. [CrossRef]
13. Svoboda, J.; Král, M.; Dendisová, M.; Matějka, P.; Pop-Georgievski, O. Unraveling the influence of substrate on the growth rate, morphology and covalent structure of surface adherent polydopamine films. *Colloids Surf. B* **2021**, *205*, 111897. [CrossRef] [PubMed]
14. Lim, J.; Zhang, S.; Heo, J.; Widanagem, M.C.D.; Ramamoorthy, A.; Kim, J. Polydopamine Adhesion: Catechol, Amine, Dihydroxyindole, and Aggregation Dynamics. *ACS Appl. Mater. Interfaces* **2024**, *16*, 31864–31872. [CrossRef] [PubMed]
15. Liebscher, J.; Mrówczyński, R.; Scheidt, H.A.; Filip, C.; Hădade, N.D.; Turcu, R.; Bende, A.; Beck, S. Structure of Polydopamine: A Never-Ending Story? *Langmuir* **2013**, *29*, 10539–10548. [CrossRef] [PubMed]
16. Delparastan, P.; Malollari, K.G.; Lee, H.; Messersmith, P.B. Direct Evidence for the Polymeric Nature of Polydopamine. *Angew. Chem. Int. Ed.* **2019**, *58*, 1077–1082. [CrossRef] [PubMed]
17. Singh, A.; Mason, T.G.; Lu, Z.; Hill, A.J.; Pas, S.J.; Teo, B.M.; Freeman, B.D.; Izgorodina, E.I. Structural elucidation of polydopamine facilitated by ionic liquid solvation. *Phys. Chem. Chem. Phys.* **2023**, *25*, 14700–14710. [CrossRef] [PubMed]
18. Hu, X.; Mao, J.; Zhang, Q.; Dong, X.; Du, H.; Wu, M.; Cheng, W.; Yang, Z. Study on the interfacial adhesion mechanism between polydopamine and coal: Experimental demonstration and molecular simulation. *Appl. Surf. Sci.* **2024**, *659*, 159947. [CrossRef]
19. Hoque, M.A.; Cossio, J.B.; Guzman, M.I. Photocatalysis of Adsorbed Catechol on Degussa P25 TiO_2 at the Air−Solid Interface. *J. Phys. Chem. C* **2024**, *128*, 17470−17482. [CrossRef] [PubMed]
20. Guo, Z.; Wang, G.; Fu, H.; Wang, P.; Liao, J.; Wanga, A. Photocatalytic degradation of methylene blue by a cocatalytic PDA/TiO_2 electrode produced by photoelectric polymerization. *RSC Adv.* **2020**, *10*, 26133. [CrossRef] [PubMed]
21. Aguilar-Ferrer, D.; Szewczyk, J.; Coy, E. Recent developments in polydopamine-based photocatalytic nanocomposites for energy production: Physico-chemical properties and perspectives. *Catal. Today* **2022**, *397–399*, 316–349. [CrossRef]
22. Sun, X.; Yan, L.; Xu, R.; Xu, M.; Zhu, Y. Surface modification of TiO_2 with polydopamine and its effect on photocatalytic degradation mechanism. *Colloids Surf. A* **2019**, *570*, 199–209. [CrossRef]
23. Kosmulski, M. The significance of the difference in the point of zero charge between rutile and anatase. *Adv. Colloid Interface Sci.* **2002**, *99*, 255–264. [CrossRef] [PubMed]
24. Tombácz, E.; Nesztor, D.; Szekeres, M.; Lewandowski, H.; Klumpp, E.; Gerencsér-Berta, R. Protolitic reactions at electrified TiO_2 P25 interface: Quantitative and thermodynamic characterization. *Molecules* **2025**, *30*, 696. [CrossRef] [PubMed]
25. Panepinto, A.; Cornil, D.; Guttmann, P.; Bittencourt, C.; Cornil, J.; Snyders, R. Fine Control of the Chemistry of Nitrogen Doping in TiO_2: A Joint Experimental and Theoretical Study. *J. Phys. Chem. C* **2020**, *124*, 17401−17412. [CrossRef]
26. Zangmeister, R.A.; Morris, T.A.; Tarlov, M.J. Characterization of polydopamine thin films deposited at short times by autoxidation of dopamine. *Langmuir* **2013**, *29*, 8619–8628. [CrossRef] [PubMed]
27. Sun, G.; Zu, F.; Koch, N.; Rappich, J.; Hinrichs, K. In situ infrared spectroscopic monitoring and characterization of the growth of polydopamine (PDA) films. *Phys. Status Solidi B* **2019**, *256*, 1800308. [CrossRef]
28. Alfieri, M.L.; Panzella, L.; Napolitano, A. Multifunctional coatings hinging on the catechol/amine interplay. *Eur. J. Org. Chem.* **2024**, *27*, e202301002. [CrossRef]
29. Nucera, A.; Guzzi, R.; Desiderio, G.; Ferraro, A.; Dal Poggetto, G.; Castriotaba, M.; Gennari, O. Size and surface properties of polydopamine nanoparticles tunable via controlled oxidation conditions. *Mater. Adv.* **2025**, *6*, 6956. [CrossRef]
30. Muccifora, S.; Castillo-Michel, H.; Barbieri, F.; Bellani, L.; Ruffini Castiglione, M.; Spanò, C.; Pradas del Real, A.E.; Giorgetti, L.; Tassi, E.L. Synchrotron Radiation Spectroscopy and Transmission Electron Microscopy Techniques to Evaluate TiO_2 NPs Incorporation, Speciation, and Impact on Root Cells Ultrastructure of Pisum sativum L. Plants. *Nanomaterials* **2021**, *11*, 921. [CrossRef] [PubMed]
31. Diebold, U. The surface science of titanium dioxide. *Surf. Sci. Rep.* **2003**, *48*, 53–229. [CrossRef]
32. Luca, I.T.; Dubois, E.; Chevalet, J.; Durand-Vidal, S. Reactivity of nanocolloidal particles γ-Fe_2O_3 at the charged interfaces. *Phys. Chem. Chem. Phys.* **2008**, *10*, 3263–3273. [CrossRef] [PubMed]
33. Giesbers, M.; Kleijn, J.M.; Cohen Stuart, M.A. The electrical double layer on gold probed by electrokinetic and surface force measurements. *J. Colloid Interface Sci.* **2002**, *248*, 88–95. [CrossRef] [PubMed]
34. Bogdan, D.; Grosu, I.; Filip, C. How thick, uniform and smooth are the polydopamine coating layers obtained under different oxidation conditions? An in-depth AFM study. *Appl. Surf. Sci.* **2022**, *597*, 153680. [CrossRef]
35. Adamczy, Z.; Sadowska, M.; Nattich-Rak, M. Quantifying Nanoparticle Layer Topography: Theoretical Modeling and Atomic Force Microscopy Investigations. *Langmuir* **2023**, *39*, 1506–15077. [CrossRef] [PubMed]
36. Marques-Moros, F.; Forment-Aliaga, A.; Pinilla-Cienfuegos, E.; Canet-Ferrer, J. Mirror effect in atomic force microscopy profiles enables tip reconstruction. *Sci. Rep.* **2020**, *10*, 18911. [CrossRef] [PubMed]

37. Kropp, J.A.; Cai, Y.; Yai, Z.; Zhu, W.; Gougousi, T. Atomic layer deposition of Al_2O_3 and TiO_2 on MoS_2 surfaces. *J. Vac. Sci. Technol. A* **2018**, *36*, 06A101. [CrossRef]
38. Park, T.; Kim, H.; Leem, M.; Ahn, W.; Choi, S.; Kim, J.; Uh, J.; Kwon, K.; Jeong, S.; Park, S.; et al. Atomic layer deposition of Al_2O_3 on MoS_2, WS_2, WSe_2, and h-BN: Surface coverage and adsorption energy. *RSC Adv.* **2017**, *7*, 884–889. [CrossRef]